applied sciences

MDPI

Article

Influence of Xenon–Fluorine–Sulfur Hexafluoride $\left(Xe^+ - F^- - SF_6^-\right)$ and Argon–Fluorine–Sulfur Hexafluoride $\left(Ar^+ - F^- - SF_6^-\right)$ Streaming on Dust Surface Potential (DSP) that Has Cairn–Tsallis Distributed Plasmas

Bahaaudin M. Raffah [1,2], A. A. Abid [3,4,*], Y. Al-Hadeethi [1,2] and H. H. Somaily [5,6]

1 Department of Physics, Faculty of Sciences, King Abdulaziz University, Jeddah 21589, Saudi Arabia
2 Lithography in Device Fabrication and Development Research Group, Deanship of Scientific Research, King Abdulaziz University, Jeddah 21589, Saudi Arabia
3 Department of Plasma Physics and Fusion Engineering, University of Science and Technology of China, Hefei 230026, China
4 National Center for Physics at QAU Campus, Shahdra Valley Road, Islamabad 44000, Pakistan
5 Research Center for Advanced Materials Science (RCAMS), King Khalid University, Abha 61413, Saudi Arabia
6 Department of Physics, Faculty of Science, King Khalid University, Abha 61413, Saudi Arabia
* Correspondence: abidaliabid1@hotmail.com; Tel.: +00-92(346)521-4088

Abstract: The dust grain surface potential is examined analytically and numerically in dusty plasmas containing negative/positive ion species by using the Cairn Tsallis (non-Maxwellian) dusty plasma. The equations for the dust-charging process are derived to solve the current balance equation for the xenon–fluorine–sulfur hexafluoride and argon–fluorine–sulfur hexafluoride plasmas. The charging process affected by plasma properties such as spectral indices α and q, in addition to positive ion streaming (U_{Ar^+} and U_{Xe^+}) and negative ion streaming (U_{F^-} and $U_{SF_6^-}$) of both types of plasmas, is examined . Our findings suggest that considering a wide range of $Xe^+ - F^- - SF_6^-$ and $Ar^+ - F^- - SF_6^-$ masses is critical for understanding plasma physics, specifically multi-component plasmas.

Keywords: dusty plasma; dust surface potential; Cairn-Tsallis distribution

check for updates

Citation: Raffah, B.M.; Abid, A.A.; Al-Hadeethi, Y.; Somaily, H.H. Influence of Xenon–Fluorine–Sulfur Hexafluoride $\left(Xe^+ - F^- - SF_6^-\right)$ and Argon–Fluorine–Sulfur Hexafluoride $\left(Ar^+ - F^- - SF_6^-\right)$ Streaming on Dust Surface Potential (DSP) that Has a Cairn–Tsallis Distributed Plasmas. *Appl. Sci.* **2022**, *12*, 11212. https://doi.org/10.3390/app122111212

Academic Editor: Emilio Martines

Received: 2 August 2022
Accepted: 8 October 2022
Published: 5 November 2022

Publisher's Note: MDPI stays neutral with regard to jurisdictional claims in published maps and institutional affiliations.

Copyright: © 2022 by the authors. Licensee MDPI, Basel, Switzerland. This article is an open access article distributed under the terms and conditions of the Creative Commons Attribution (CC BY) license (https://creativecommons.org/licenses/by/4.0/).

1. Introduction

During the last few decades, a notable improvement has been made regarding the dusty (complex) plasmas having negatively/positively charged dust grains, ion, electron, and neutral plasmas components. The examples of dusty plasma in astrophysics and space systems are asteroid regions, interstellar media, interplanetary spaces, dark molecular clouds, accretion disks, earth's surroundings, and industry plasmas [1–4]. Inertia is produced by the dust particle mass, and the restoring force is provided by the pressure of electrons/ions in the dust-acoustic (DA) mode. Rao et al. [5] studied a dusty plasma (unmagnetized) and theoretically predicted the low-phase-velocity dust acoustic (DA) waves (in comparison to both electron as well as ion thermal velocities) . The laboratory experiments [6] demonstrated some nonlinear features of dust acoustic waves. Dust grains are embedded in a surrounding plasma and radiative background under typical experimental settings. Because of the charge they carry, they interact with electrons and ions. Photoelectric emission, due to collision with electrons/ions, and secondary emission are some of the competing processes that charge dust grains, depending on local conditions [6]. Massive dust particles can accumulate a huge number of plasma electrons with high mobility, resulting in a dust particle with a negative charge. Consequently, the positive ion

current increases and the electron current decreases as a result of the negative dust-surface potential. The steady-state of the electron current (I_e) and ion current (I_i) is $|I_e| = |I_i|$, which establishes the equilibrium dust charge. The bombardment of electrons and positive ions was postulated to be the cause of dust charge in 1994 [7], when DSP was theoretically and experimentally investigated . These studies have been further expanded [8,9] to emphasize the importance of negatively charged ions in Maxwellian/non-Maxwellian-distributed plasmas.

There are several plasma events in space, such as the interstellar medium, ionosphere, thermosphere, planetary magnetosphere, ionosphere, and magnetosheaths, and the non-Maxwellian velocity distribution is frequently observed [10–12]. A novel distribution, developed to describe super-thermal particles detected by the Viking [13] and Freja-satellite [14], has been presented by Cairns et al. [15]. It has been expressed as a parameter alpha (α) that calculates the variance from the Maxwellian to non-Maxwellian. As a result, it has **b**een observed that in the presence of non-thermal electrons, the characteristics of ion-sound-solitary waves can alter, resulting in nonlinear solitary waves with either an augmented or depleted density. The Cairns model has since been used in a number of studies [16–19]. Verheest and Pillay, for example, studied large-amplitude dust-acoustic (DA) solitary structures in negatively dusty plasmas, in either non-thermal ions or electrons [20] . Later, [21] further looked into large ion-acoustic (IA) solitary structures and double layers (DL) that have positive ions as well non-**t**hermal electrons plasmas. Mamun and colleagues have also looked at the combined effect of positively dust grains and non-thermal electrons in dust–IA solitary waves and the presence of non-thermal ions in DA waves [16]. In recent years, statistically non-extensive events using the Boltzmann–Gibbs–Shannon (BGS) entropic dimension deviation have received much attention. In statistical mechanics, large thermodynamical quantities are proportional to the mass of matter present, e.g., the particle number (N), the volume (V), the magnetization (M), the internal energy (E), and so on. The temperature (T), pressure (P), and chemical potential (μ) are non-extensive quantities that are not dependent on the mass of matter. Furthermore, the ratio of the extensive variables yields a non-extensive variable, for example, the number density = (particle number/volume), which is the proportionality of the number of particles to the system's volume. Renyi proposed and Tsallis [22] researched a suitable BGS entropy, statistically under equilibrium**.** The nonlinear and non-extensive situation of the entropies was continued by Tsallis; the entropic (spectral) index q depicts the level of non-extensivity of the assumed framework. There are two major physical zones that can be identified: the $-1 < q \leq 1$ region, which has all velocities, and $q \geq 1$, in which the plasma species distribution-function capacity indicates a thermal cut-off on the most extreme quality considered: the particles' velocity [23].

Negative ions' impact in space areas [24] and in the laboratory plasmas [25] was discovered in the earth's mesosphere, the ionosphere's D zone, and the sun's photosphere. The dynamics of IA dispersive waves have also been observed with negative ions [26]. Ichiki et al. [27] looked at the parameters of IA waves in positive-/negative-ion plasma elements and found primary modes. They have demonstrated that in $Xe^+ - F^- - SF_6^-$ plasma, two modes exist considering the values of the electron temperature and ion temperature, and they also occurr in one mode in $Ar^+ - F^- - SF_6^-$ plasma, regardless of the multi-ions temperatures . Ichiki et al. [28] studied the slow mode of IA waves with various features utilizing the $Xe^+ - F^-$ plasmas in two distinct DP devices. Later research looked at the IAWs in $Xe^+ - F^- - SF_6^-$ and $Ar^+ - F^- - SF_6^-$ plasma species, revealing that this work will help with the analysis of dusty plasmas with negative ions. By using $Ar^+ - Xe^+$, the heavy and light ion modes have been studied in lab plasma [29]. In addition to the negative ion plasma employed in the labs [30], sulfur hexafluoride (SF_6) gas has been employed to generate negative ions. It has been also discovered using mass spectrometry in Ar/SF_6 plasma created in DP devices in which Ar^+, F^-, and SF_6 were present for the sufficiently high negative ion to positive ion density ratios [27], and experiments were also conducted using such plasmas [27] . In the current paper, we will analyze the $Xe^+ - F^- - SF_6^-$ and

$Ar^+ - F^- - SF_6^-$ dusty plasma and do numerical computations using the static negative dust particle. These negative ions are a form of plasma species that can arise naturally or be infused from an outside source in the space plasma and lab plasmas [31]. The control of an electrode in deposition and etching plasmas [32], the development of voids [33], and the extraction of negative ion electrode sources [34] are all dependent on negative ions. The DSP was previously [35] calculated using non-Maxwellian currents due to multi ions for dust particles that are negatively charged. We have studied the $Xe^+ - F^- - SF_6^-$ and the $Ar^+ - F^- - SF_6^-$ plasmas. To investigate the influence of plasma characteristics, we used numerical analysis on the negatively charged DSP. We noted the effects of the spectral indices α and q, positive ion streaming (U_{Ar^+} and U_{Xe^+}), and negatively ion streaming (U_{F^-} and $U_{SF_6^-}$) on DSP for both types of plasmas .

The rest of this paper is divided into the following sections: we investigate the generalized Cairn–Tsallis (q, α)-distribution function in Section 2. In Section 3, we calculate the DSP for $Xe^+ - F^- - SF_6^-$ plasma. In Section 4, we have derived the DSP for $Ar^+ - F^- - SF_6^-$ plasma utilizing the same method of analysis. The Numerical results and discussion for the type of plasmas are studied in Section 5. Finally, in Section 6, a summary of the study's significant findings is presented.

2. Cairns–Tsallis (q, α)-Distribution Function

The 3-D (q, α)-distribution function, which is particularly the combination of the Cairns–Tsallis distribution, is defined as [36]

$$f_{CT}(\mathbf{V}_j) = D_{q\alpha}\left(\frac{2\pi}{1-q}\right)^{-\frac{3}{2}}\left(\frac{T_j}{m_j}\right)^3\left(1+\alpha\frac{m_j^2V_j^4}{T_j^2}\right)\left[1-(q-1)\frac{m_jV_j^2}{2T_j}\right]^{(q-1)^{-1}}, \quad (1)$$

where T_j, m_j, and V_j are the temperature, mass, and velocity of jth plasma particles ($j = e$ is for the electrons; Xe^+ and Ar^+ are for the positive ions; SF_6^- and F^- are the negative ions (and the letter d stands for negative charge dust grains); q and α are the spectral indexes, associated with non-extensivity and the quantity of non-thermal electrons, and positive/negative ions, respectively. Here, $D_{q\alpha}$ is a constant of normalization expressed by [37].

$$\left.\begin{aligned} C_{q\alpha} &= \left[\frac{(1-q)^2\Gamma\left(\frac{1}{1-q}\right)}{\Gamma\left(\frac{1}{1-q}-\frac{5}{2}\right)\left[3\alpha+(1-q)^2\left(\frac{1}{1-q}-\frac{5}{2}\right)\left(\frac{1}{1-q}-\frac{3}{2}\right)\right]}\right] \quad \text{for} -1 < q \leq 1, \\ C_{q\alpha} &= \left[\frac{(1-q)^2\Gamma\left(\frac{5}{2}+\frac{1}{1-q}\right)\left(\frac{3}{2}+\frac{1}{q-1}\right)\left(\frac{5}{2}+\frac{1}{q-1}\right)}{\Gamma\left(1+\frac{1}{q+1}\right)\left[3\alpha+(q-1)^2\left(\frac{3}{2}+\frac{1}{q-1}\right)\left(\frac{5}{2}+\frac{1}{q-1}\right)\right]}\right] \text{ for } \quad q \geq 1, \end{aligned}\right\} \quad (2)$$

Γ is called the Gamma function. Both values of $C_{q\alpha}$ correspond to the Cairns distribution in the limit $q \to 1$ [15], and the (q, α)-distribution simplifies to a pure Tsallis distribution for $\alpha = 0$ [22]. The (q, α)-distribution reduces to the Maxwellian distribution exactly in the case of $\alpha = 0$ and $q \to 1$. It is watched that the real Tsallis (q)-distribution function carries on distinctively in the limits, $q > 1$ and $-1 < q < 1$ [23]. As in the previous extent, the real T-sallis distribution function is non-zero for the complete velocities limit $-\infty$ to $+\infty$, and it shows the high energy tail because of an abundance of super-thermal species. **These** standards, on a basic level, are like a power-law or $\kappa-$distribution function .

3. Dust-Surface Potential (DSP) with $Xe^+ - F^- - SF_6^-$ Plasma

For xenon–fluorine–sulfur hexafluoride $\left(Xe^+ - F^- - SF_6^-\right)$ plasmas, two modes exist depending on the temperatures of the electrons and ions. We investigate a non-Maxwellian complex plasma that has electrons, positive ions (Xe^+), two negative ions (SF_6^- and F^-), and negatively charged dust particles as constituents. While in balance, the charge-neutrality precondition requires $n_e - Z_{Xe^+}n_{Xe^+} + Z_{F^-}n_{_{F^-}} + Z_{SF_6^-}n_{SF_6^-} - q_dn_d/e$, where n_s is the sth species of the unperturbed number density ($s = e$ stands for electrons; Xe^+ is the Xenon

ions; $F^-$and SF_6^- stand for fluorine and sulfur ions, respectively; and d stands for charged (negatively) dust particles). Z_{Xe^+}, Z_{F^-}, and $Z_{SF_6^-}$ stand for the charging state of the argon, fluorine, and sulfur hexafluoride, respectively, and q_d stands for the charge on the dust grains. When q_d =constant, the electrons, the positive ion, and the two negative ions in the (q, α)-distributional currents may be represented, [38]

$$I_e^{q\alpha} + I_{Xe^+}^{q\alpha} + I_{F^-}^{q\alpha} + I_{SF_6^-}^{q\alpha} = 0, \tag{3}$$

with

$$\sigma_j^d = \pi r_d^2 \left(1 - \frac{2q_j\phi_d}{m_j V_j^2}\right), \tag{4}$$

$$I_j^{q\alpha} = q_j \int V_j \sigma_j^d f_{CT}(\mathbf{V}_j) d^3\mathbf{V}_j. \tag{5}$$

σ_j^d stands for the cross-section for charging interactions among dust particles and plasmas constituents of charge q_j, and ϕ_d is the DSP of radius r_d. To continue, we integrate over the $f_{CT}(\mathbf{V}_j)$ to simplify Equation (2). In spherical-coordinates, write the volume element as $d^3\mathbf{V}_j = V_j^3 dV_j d\mu d\phi$ to obtain the currents owing to electrons, positive ions, and the two negative ions due to negative charge dust particles [38], respectively.

$$I_e^{q\alpha} = -\sqrt{2^3}\pi r_d^2 \exp\left(\frac{\chi_{q\alpha}}{\tau_{q\alpha}} \frac{e\phi_d}{m_e V_{Te}^2}\right) V_{Te} n_e \tau_{q\alpha} C, \tag{6}$$

$$I_{Xe^+}^{q\alpha} = \sqrt{2^3}\pi r_d^2 \left\{1 - \frac{\chi_{q\alpha}}{\tau_{q\alpha}} \frac{e\phi_d}{m_{Xe^+} V_{Xe^+}^2}\right\} Z_{Xe^+} V_{Xe^+} e n_{Xe^+} \tau_{q\alpha} C, \tag{7}$$

and

$$I_{F^-}^{q\alpha} = -\sqrt{2^3}\pi r_d^2 \left\{1 + \frac{\chi_{q\alpha}}{\tau_{q\alpha}} \frac{Z_{F^-} e\phi_d}{m_{F^-} V_{F^-}^2}\right\} Z_{F^-} V_{F^-} e n_{F^-} \tau_{q\alpha} C, \tag{8}$$

$$I_{SF_6^-}^{q\alpha} = -\sqrt{2^3}\pi r_d^2 \left\{1 + \frac{\chi_{q\alpha}}{\tau_{q\alpha}} \frac{Z_{SF_6^-} e\phi_d}{m_{SF_6^-} V_{SF_6^-}^2}\right\} Z_{SF_6^-} V_{SF_6^-} e n_{SF_6^-} \tau_{q\alpha} C, \tag{9}$$

and

$$C = \left(\frac{1}{1-q}\right)^{-\frac{3}{2}} \left[\frac{(1-q)^2 \Gamma\left(\frac{1}{1-q}\right)}{\Gamma\left(\frac{1}{1-q} - \frac{5}{2}\right)\left[3\alpha + \left(\frac{1}{1-q} - \frac{3}{2}\right)\left(\frac{1}{1-q} - \frac{5}{2}\right)(1-q)^2\right]}\right], \text{for } -1 < q \leq 1,$$

where $\tau_{q\alpha} = \left[(6 + 24\alpha - 17q + 12q^2)/(-6q + 29q^2 - 46q^3 + 24q^4)\right]$ and $\chi_{q\alpha} = 1/q + 8\alpha/(2q - 7q^2 + 6q^3)$. The DSP of a negatively charged dust particle can be written as by substituting Equations (6)–(9) into Equation (3).

$$\begin{aligned}
&\sqrt{U_{Xe^+}} - \frac{\chi_{q\alpha}}{\tau_{q\alpha}} \frac{Z_{Xe^+}\psi}{\sqrt{U_{Xe^+}}} - \varepsilon_1 \left(1 - \Delta_1 \frac{Z_{F^-}}{Z_{Xe^+}} - \Delta_2 \frac{Z_{SF_6^-}}{Z_{Xe^+}} + Z_{Xe^+}\psi P_d\right) \exp\left(\frac{\chi_{q\alpha}}{\tau_{q\alpha}}\psi\right) \\
&= \Delta_1 \eta_1 \sqrt{U_{F^-}} \frac{Z_{F^-}}{Z_{Xe^+}} \left(1 + \frac{\chi_{q\alpha}}{\tau_{q\alpha}} \frac{Z_{F^-}\psi}{U_{F^-}}\right) + \Delta_2 \eta_{2^-} \sqrt{U_{SF_6^-}} \frac{Z_{SF_6^-}}{Z_{Xe^+}} \left(1 + \frac{\chi_{q\alpha}}{\tau_{q\alpha}} \frac{Z_{SF_6^-}\psi}{U_{SF_6^-}}\right),
\end{aligned} \tag{10}$$

$$\Delta_1 = \frac{n_{F^-}}{n_{Xe^+}}, \Delta_2 = \frac{n_{SF_6^-}}{n_{Xe^+}}, \ \eta_1 = \left(\frac{m_{Xe^+}}{m_{F^-}}\right)^{1/2}, \ \eta_2 = \left(\frac{m_{Xe^+}}{m_{SF_6^-}}\right)^{1/2}, \tag{11}$$

$$U_{F^-} = \frac{m_{_{F^-}} V_{F^-}^2}{2T_e}, U_{_{SF_6^-}} = \frac{m_{_{SF_6^-}} V_{_{SF_6^-}}^2}{2T_e}, U_{Xe^+} = \frac{m_{_{Xe^+}} V_{Xe^+}^2}{2T_e}, \text{ and } \varepsilon_1 = \left(\frac{m_{Xe^+}}{m_e}\right)^{1/2}. \quad (12)$$

Normalized DSP is denoted by $\psi = e\phi_d/T_e$, and the normalized dust number density by $P_d = 4\pi n_d r_d \rho_0^2$ with $\rho_0 = \sqrt{T_e/(4\pi n_{Xe^+} Z_{Xe^+}^2 e^2)}$. It has been observed that for significant conditions for $\alpha = 0$ and $q = 1$, $\chi_{q\alpha} = 1$ and $\tau_{q\alpha} = 1$, and by using one species of negative ion, Equation (10) agrees to the previous Equation (6) of Ref. [8], which shows that the DSP in a Maxwellian dusty plasma has negative ion streaming . Equation (10) is numerically solvable to investigate the relationship between ψ and P_d.

4. Dust Grain Surface Potential (DSP) with $Ar^+ - F^- - SF_6^-$ Plasmas

When we use different forms of plasmas $Ar^+ - F^- - SF_6^-$, the Ar^+ current can be stated as follows:

$$I_{Ar^+}^{q\alpha} = \sqrt{2^3}\pi r_d^2 \left\{1 - \frac{\chi_{q\alpha}}{\tau_{q\alpha}} \frac{e\phi_d}{m_{Ar^+} V_{Ar^+}^2}\right\} Z_{Ar^+} V_{Ar^+} e n_{_{Ar^+}} \tau_{q\alpha} C, \quad (13)$$

Using the same technique as in Section 3, when we substitute Equations (6), (8), (9), and (13) into (3), we obtain

$$\sqrt{U_{Ar^+}} - \frac{\chi_{q\alpha}}{\tau_{q\alpha}} \frac{Z_{Ar^+}\psi}{\sqrt{U_{Ar^+}}} - \varepsilon_2 \left(1 - \Delta_3 \frac{Z_{F^-}}{Z_{Ar^+}} - \Delta_4 \frac{Z_{SF_6^-}}{Z_{Ar^+}} + Z_{Ar^+}\psi P_d\right) \exp\left(\frac{\chi_{q\alpha}}{\tau_{q\alpha}}\psi\right)$$
$$= \Delta_3 \eta_3 \sqrt{U_{F^-}} \frac{Z_{F^-}}{Z_{Ar^+}} \left(1 + \frac{\chi_{q\alpha}}{\tau_{q\alpha}} \frac{Z_{F^-}\psi}{U_{F^-}}\right) + \Delta_4 \eta_{4^-} \sqrt{U_{SF_6^-}} \frac{Z_{SF_6^-}}{Z_{Ar^+}} \left(1 + \frac{\chi_{q\alpha}}{\tau_{q\alpha}} \frac{Z_{SF_6^-}\Psi}{U_{SF_6^-}}\right), \quad (14)$$

where

$$\Delta_3 = \frac{n_{F^-}}{n_{Ar^+}}, \Delta_4 = \frac{n_{_{SF_6^-}}}{n_{Ar^+}}, \eta_{3^-} = \left(\frac{m_{Ar^+}}{m_{F^-}}\right)^{1/2}, \eta_4 = \left(\frac{m_{_{Ar^+}}}{m_{_{SF_6^-}}}\right)^{1/2}, \quad (15)$$

$$U_{Ar^+} = \frac{m_{_{Ar^+}} V_{Ar^+}^2}{2T_e}, \text{ and } \varepsilon_2 = \left(\frac{m_{Ar^+}}{m_e}\right)^{1/2}. \quad (16)$$

Equation (14) depicts a relationship between the DSP and P_d in the presence of Ar^+ ions is dipicted in Equation (14). By applying a limit on spectral indices $\alpha = 0$ and $q = 1$, the value of $\chi_{q\alpha} = 1$ and $\tau_{q\alpha} = 1$, and Equation (14), Equation (6) of Ref. [8] uses only one species of negative ion, which shows that the DSP in a Maxwellian dusty plasma has negative ion streaming . Equation (14) can be numerically solved to investigate the relationship between the DSP and the $P_{\mathbf{d}}$.

5. Numerical Results and Discussion

We have displayed the (q, α)-distribution [15] in Equation (1) for various values of spectral index α and q for numerical demonstration. The spectral indices q and α represent the influence on the tail of super thermal particles and the shoulder of the velocity-disturbed graph, respectively. Figure 1a,b are plotted for condition $-1 < q \leq 1$. The effect of different values of the spectral index $\alpha(0.1, 0.15, 0.2)$ for the fixed value of q (=0.7) is shown in Figure 1a. α illustrates the high-energy plasma elements on the shoulder of the graph. The distribution function $f_{CT}(V_j)$ as a function of V_j is plotted for different values of $\alpha(0.1, 0.15, 0.2)$ at a fixed value of q (=0.9), as shown in Figure 1b. This figure shows that (q, α)-distributed reduces to Maxellian at $q = 0.9$ and $\alpha = 0$. Figure 1c,d depict the (q, α)-distribution for different values of non-extensive spectral index $q \geq 1$. It is observed that for increasing values of α, the prominent effects of distribution are shown on the top shoulders, while the magnitude of the velocity distribution curves are nearly the same on the initial and end regions. Figure 1c,d show the values of the non-extensive spectral index q. It

is discovered that as the value of increases, the prominent effects of plasma species are observed on the top shoulders but have no effect on the tails of velocity distribution curves.

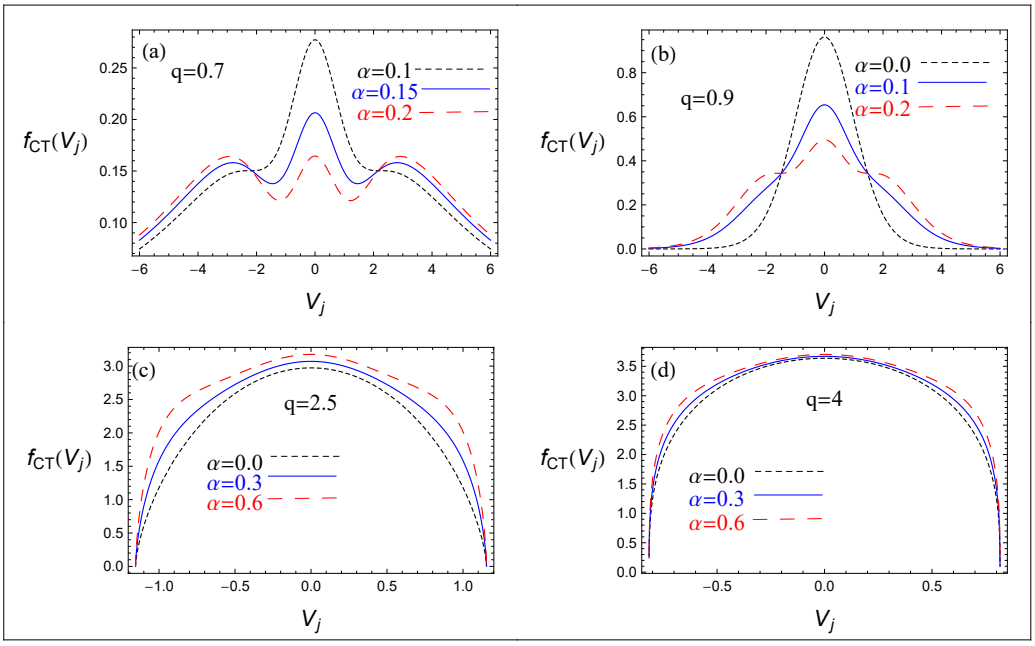


Figure 1. (Color online) normalized (q, α)-distribution function (**a**) $\alpha(0.1, 0.15, 0.2)$ with $q = 0.7$ (**b**) $\alpha(0.0, 0.1, 0.2)$ with $q = 0.9$ (**c**) $\alpha(0.0, 0.3, 0.6)$ with $q = 2.5$ and (**d**) $\alpha(0.0, 0.3, 0.6)$ with $q = 4$.

In the framework of Cairn–Tsallis-distributed dusty plasmas, the (10) and (14) are numerically solved, considering the typical properties of laboratory plasmas. In recent work, we evaluated the DSP (ψ), versus dust-density parameter P_d, for species $Xe^+ - F^- - SF_6^-$ and $Ar^+ - F^- - SF_6^-$. Furthermore, the mass of ions associated with Xe^+ and Ar^+ is composed of $131m_P$ and $40m_P$, respectively, where m_p is mass of a proton. The mass ratios for $Xe^+ - F^- - SF_6^-$ and $Ar^+ - F^- - SF_6^-$ are η_1, η_2, η_3, and η_4 are $(131/19)^{1/2}$, $(131/146)^{1/2}$, $(40/19)^{1/2}$, and $(40/146)^{1/2}$, respectively. Previously, the IA waves in plasmas (multi-ions) were explored numerically and experimentally [18], with the two kinds of negative ions. Figure 2 illustrates the DSP versus dust-density parameter P_d for the various values of spectral index $\alpha(0.0, 0.01, 0.02)$; the fixed values of spectral index q and the values of other parameters include $Z_{Xe} = Z_F = Z_{Ar^+} = Z_{SF} = 1$, $U_{Xe^+} = U_{Ar^+} = U_{F^-} = U_{SF_6^-} = U_{Xe^+} = 0.5$, $\Delta_1 = \Delta_2 = \Delta_3 = \Delta_4 = 0.4$, $\varepsilon_1 = (131/0.00055)^{1/2}$, $\varepsilon_2 = (40/0.00055)^{1/2}$. It is shown in Figure 2a that the magnitude of DSP varies directly with the α, by taking into account the $Xe^+ - F^- - SF_6^-$ plasmas (using Equation (10)). The same effect spectral index α is observed in $Ar^+ - F^- - SF_6^-$ plasmas (using Equation (14)). Furthermore, the dust **s**urface potential in $Xe^+ - F^- - SF_6^-$ is frequently larger than in $Ar^+ - F^- - SF_6^-$, owing to the higher mass of Ar^+. For spectral index α with other parameters held constant, the dust DSP demonstrates almost monotonic behavior.

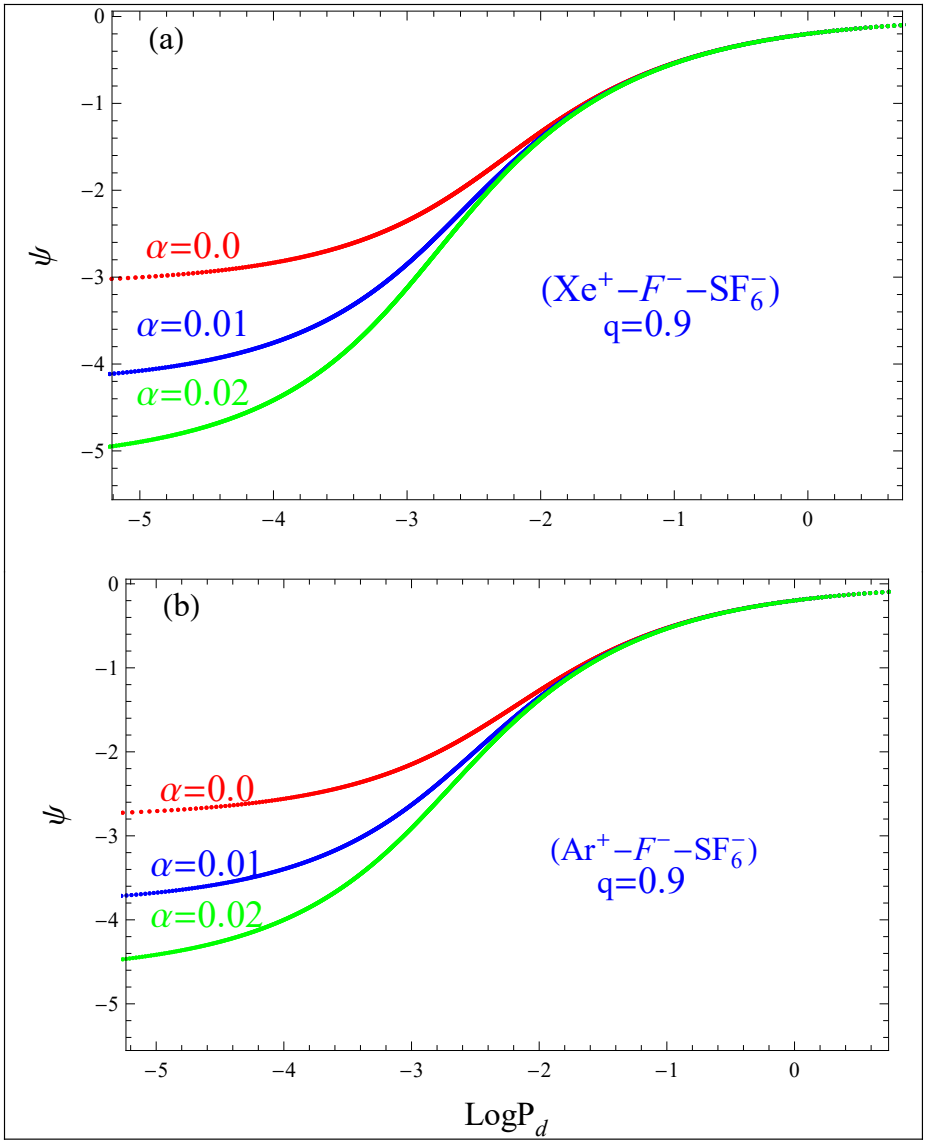


Figure 2. (Color online) ψ versus P_d for $\alpha(0.0, 0.01, 0.02)$ with $q = 0.9$; (**a**) xenon–fluorine–sulfur hexafluoride as given in Equation (10) (**b**) for argon–fluorine–sulfur hexafluoride plasma as given in Equation (14) .

Using Equations (10) and (14), we show the profiles of the DSP vs. dust parameter P_d for both types of plasmas with different values of spectral index q (=0.90.05,1.0) and a fixed value of alpha (=0.01) for both types of plasmas in Figure 3a,b, respectively. Both Figure 3a,b show that as the value of q increases, the dust-surface potential drops.

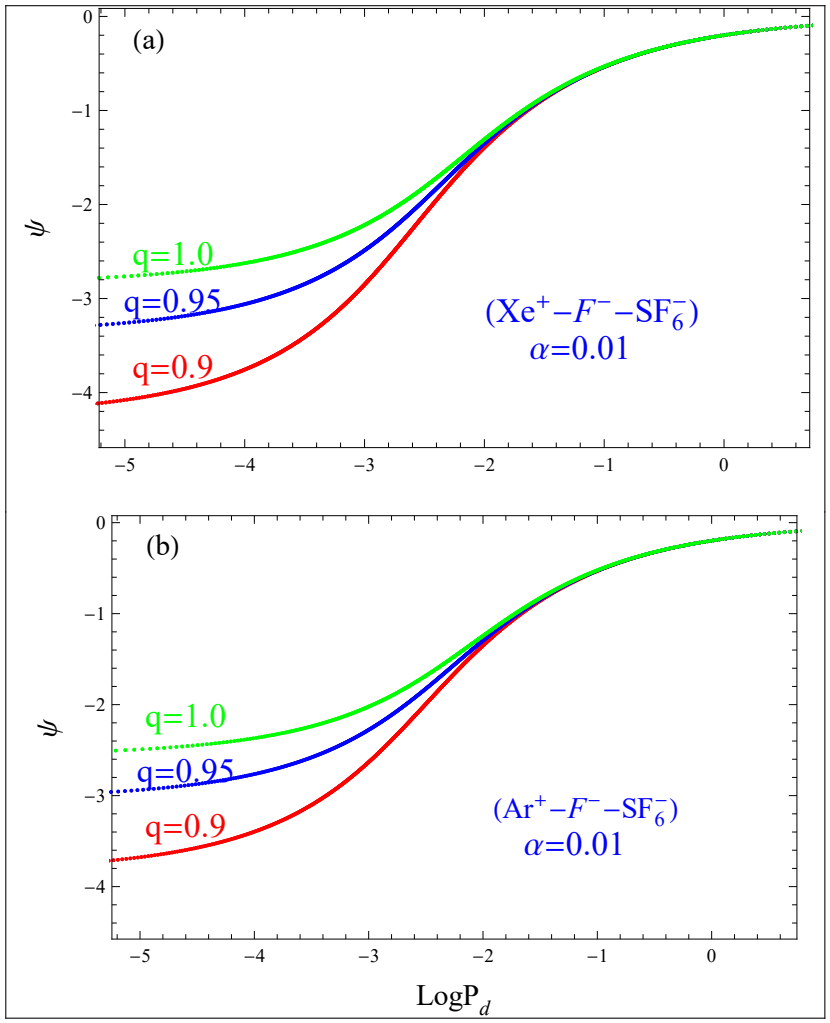


Figure 3. (Color online) ψ versus P_d for $q(0.9, 0.95, 1.0)$ with $\alpha = 0.01$; (**a**) xenon–fluorine–sulfur hexafluoride as given in Equation (10) (**b**) for argon–fluorine–sulfur hexafluoride plasma as given in Equation (14) .

In Figure 4a,b, we illustrate the profiles of the DSP versus dust parameter P_d with different values $(0.1, 0.4, 0.8)$ of Xenon ion streaming velocity $[U_{Xe^+} = m_{_{Xe^+}} V_{Xe^+}/2T_e]$ and Argon ion streaming velocity $[U_{Ar^+} = m_{_{Ar^+}} V_{Ar^+}/2T_e]$ with a fixed value of spectral indices α $(= 0.02)$ and $q(= 0.95)$ by using Equations (10) and (14), respectively. We observed that by increasing the values of $U_{Xe^+}(0.1, 0.4, 0.8)$ and $U_{Ar^+}(0.1, 0.4, 0.8)$, the magnitude of DSP increases, while the value of negative streaming velocity stays the same. In Figure 5a–d, the DSP curves are plotted as a versus P_d for different cases of negative ions (U_{F^-} and $U_{_{SF_6^-}}$) for both types of plasma.

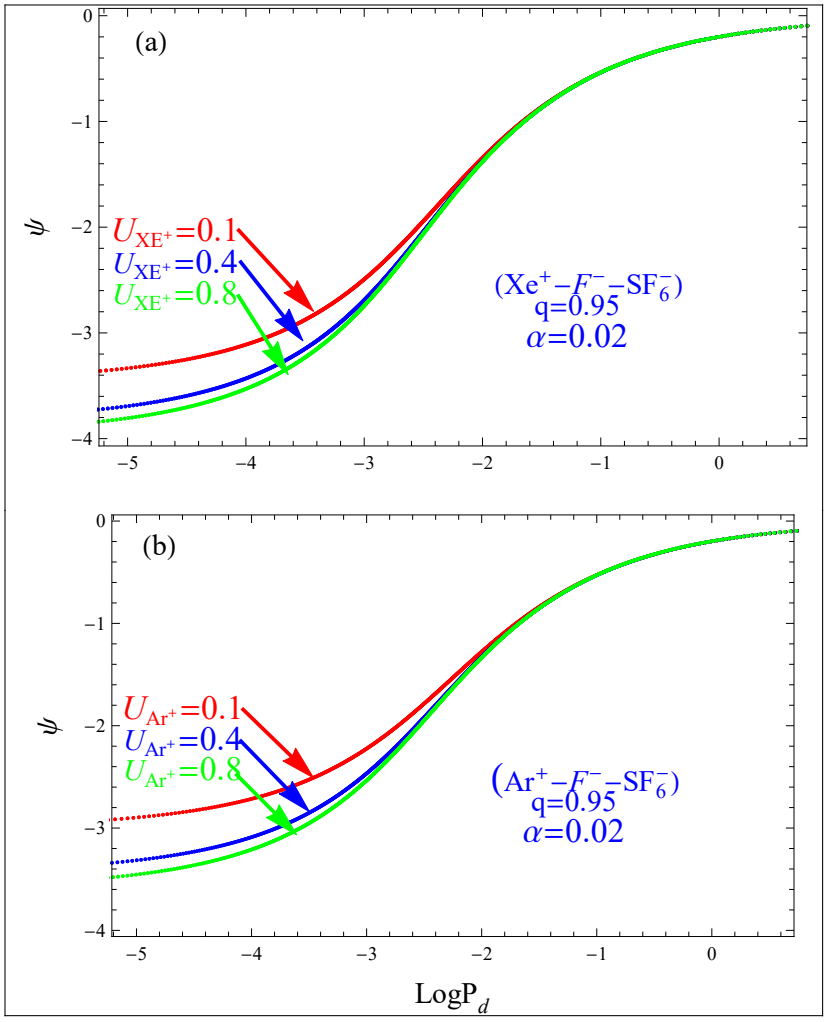


Figure 4. (Color online) ψ versus P_d (**a**) for $U_{Xe^+}(0.1, 0.4.0.8)$ with $q = 0.95$ and $\alpha = 0.02$, for xenon–fluorine–sulfur hexafluoride as given in Equation (10) (**b**) for $U_{Ar^+}(0.1, 0.4.0.8)$ with $q = 0.95$ and $\alpha = 0.02$ for argon–fluorine–sulfur hexafluoride plasma as given in Equation (14).

Figure 5a shows the variation of the DSP against the P_d of $Xe^+ - F^- - SF_6^-$ plasma for different values of $U_{F^-}(= 0.1, 0.4, 0.8)$, with $\alpha = 0.02$ and $q = 0.95$ kept the same. It is observed that the DSP increases by increasing the values of streaming fluorine ion. Figure 5b examines the streaming effect of $U_{SF_6^-}$ on dust potential with U_{F^-}, and the remainder of the parameters are the same as in Figure 2a. The streaming influence of $U_{SF_6^-}$ on DSP is the same as U_{F^-}, but the difference between the curves of $U_{SF_6^-}$ is smaller than U_{F^-}. The effects of U_{F^-} and $U_{SF_6^-}$ on DSP for $Ar^+ - F^- - SF_6^-$ plasmas are shown in Figure 5c,d. The non-monotonic change in dust potential can also be seen in Figure 5c,d, with comparable consequences to those shown in Figure 5a,b. The physical significance for the observed trend is mainly due to the positive/negative ion streaming that gradually increases the relative potential (ψ) of ions as well as the negative charge dust particles. The dust-surface potential increases with the increase in ion velocity but decreases with the collisions of ions with dust particles.

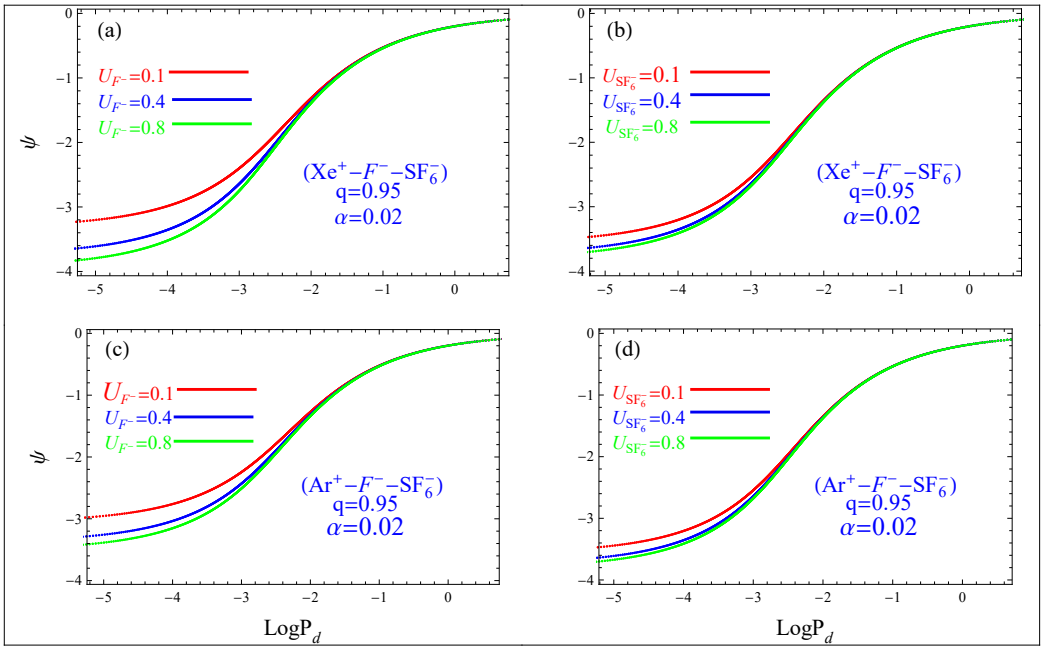


Figure 5. (Color online) ψ versus P_d, (**a**) for $U_{F^-}(0.1, 0.4.0.8)$ with $q = 0.95$ and $\alpha = 0.02$, (**b**) $U_{SF_6^-}(0.1, 0.4.0.8)$ with $q = 0.95$ and $\alpha = 0.02$ for xenon–fluorine–sulfur hexafluoride as given in Equation (10) (**c**) for $U_{F^-}(0.1, 0.4.0.8)$ with $q = 0.95$ and $\alpha = 0.02$, (**d**) $U_{SF_6^-}(0.1, 0.4.0.8)$ with $q = 0.95$ and $\alpha = 0.02$ for argon–fluorine–sulfur hexafluoride plasma as given in Equation (14).

6. Conclusions

In the present work, we have studied a DSP variation by taking into consideration the positive/negative ion streaming in the presence of Cairns–Tsallis distributed plasmas. For the $Xe^+ - F^- - SF_6^-$ and $Ar^+ - F^- - SF_6^-$ plasma species, the DSP for the negatively charged dust particles is calculated numerically and analytically. In the contest of Cairns–Tsallis plasma, the equations for the DSP from the current balance equation are determined analytically by taking into consideration the electrons, negative ions (F^- and SF_6^-), and positive ions (Xe^+ and Ar^+) for the charged dust grains. (i) The magnitude of dust-surface potential ($|\Psi|$) increases with an increase in the spectral index α, positive ion streaming velocity (U_{Ar+} and U_{Xe+}), and negative ion streaming velocity (U_{F^-} and $U_{SF_6^-}$). (ii) The magnitude of dust-surface potential ($|\Psi|$) diminishes and approaches the Maxwellian case when the value of the spectral index q is increased. The key parameters have a significant impact on the DSP, for example, the spectral indices α and q, positive ion streaming (U_{Ar^+} and U_{Xe^+}), and negative ion streaming (U_{F^-} and $U_{SF_6^-}$) of both types of plasmas. For the $Xe^+ - F^- - SF_6^-$ and $Ar^+ - F^- - SF_6^-$ plasma species, the numerical outcomes show both monotonic as well as non-monotonic profiles of the DSP. Finally, we come to the conclusion that the results of our investigations should be important for understanding dust-charging processes, computing dust-charge variation, and comparing dust-surface potential in low-temperature plasma species that contain electrons as well as positive and negative ions and by using the Cairns–Tsallis distribution function.

Author Contributions: Data curation, B.M.R. and A.A.A.; Formal analysis, B.M.R. and A.A.A.; Methodology, B.M.R. and A.A.A.; Writing—original draft, Y.A.-H. and H.H.S.; Writing—review & editing, Y.A.-H. and H.H.S. All authors have read and agreed to the published version of the manuscript.

Funding: The Deanship of Scientific Research (DSR) at King Abdulaziz University (KAU), Jeddah, Saudi Arabia has funded this project, under grant no. (RG-17-130-43).

Institutional Review Board Statement: Not applicable.

Informed Consent Statement: Not applicable.

Data Availability Statement: Not applicable.

Conflicts of Interest: The authors declare no conflict of interest.

References

1. Shukla, P.K.; Mamun, A.A. *Introduction to Dusty Plasma Physics*; IOP Publishing Ltd.: Bristol, UK, 2002.
2. Horanyi, M.; Mendis, D.A. Trajectories of charged dust grains in the cometary environment. *Astrophys. J.* **1985**, *294*, 357–368. [CrossRef]
3. Goertz, C.K. Dusty plasmas in the solar system. *Rev. Geophys.* **1989**, *27*, 271–292. [CrossRef]
4. Fortov, V.E.; Ivlev, A.V.; Khrapak, S.A.; Khrapak, A.G.; Morfill, G.E. Complex (dusty) plasmas: Current status, open issues, perspectives. *Phys. Rep.* **2005**, *421*, 1–103. [CrossRef]
5. Rao, N.N.; Shukla, P.K.; Yu, M.Y. Dust-acoustic waves in dusty plasmas. *Planet. Space Sci.* **1990**, *38*, 543–546. [CrossRef]
6. Barkan, A.; Merlino, R.L.; D'angelo, N. Laboratory observation of the dust-acoustic wave mode. *Phys. Plasmas* **1995**, *2*, 3563–3565. [CrossRef]
7. Barkan, A.; D'angelo, N.; Merlino, R.L. Charging of dust grains in a plasma. *Phys. Rev. Lett.* **1994**, *73*, 3093. [CrossRef]
8. Mamun, A.A.; Shukla, P.K. Charging of dust grains in a plasma with negative ions. *Phys. Plasmas* **2003**, *10*, 1518–1520. [CrossRef]
9. Abid, A.A.; Ali, S.; Muhammad, R. Dust grain surface potential in a non-Maxwellian dusty plasma with negative ions. *J. Plasma Phys.* **2013**, *79*, 1117–1121. [CrossRef]
10. Vasyliunas, V.M. Low-energy electrons on the day side of the magnetosphere. *J. Geophys. Res.* **1968**, *73*, 7519–7523. [CrossRef]
11. Hellberg, M.A.; Mace, R.L.; Baluku, T.K.; Kourakis, I.; Saini, N.S. Comment on "Mathematical and physical aspects of Kappa velocity distribution" [Phys. Plasmas 14, 110702 (2007)]. *Phys. Plasmas* **2009**, *16*, 094701. [CrossRef]
12. Kourakis, I.; Sultana, S.; Hellberg, M.A. Dynamical characteristics of solitary waves, shocks and envelope modes in kappa-distributed non-thermal plasmas: An overview. *Plasma Phys. Control. Fusion* **2012**, *54*, 124001. [CrossRef]
13. Bostrom, R. Observations of weak double layers on auroral field lines. *IEEE Trans. Plasma Sci.* **1992**, *20*, 756–763. [CrossRef]
14. Dovner, P.O.; Eriksson, A.I.; Boström, R.; Holback, B. Freja multiprobe observations of electrostatic solitary structures. *Geophys. Lett.* **1994**, *21*, 1827–1830. [CrossRef]
15. Cairns, R.A.; Mamum, A.A.; Bingham, R.; Boström, R.; Dendy, R.O.; Nairn, C.M.; Shukla, P.K. Electrostatic solitary structures in non-thermal plasmas. *Geophys. Res. Lett.* **1995**, *22*, 2709–2712. [CrossRef]
16. Mamun, A.A. Rarefactive ion-acoustic electrostatic solitary structures in nonthermal plasmas. *Eur. Phys. J. D-At. Opt. Plasma Phys.* **2000**, *11*, 143–147. [CrossRef]
17. Jukui, X. Modulational instability of ion-acoustic waves in a plasma consisting of warm ions and non-thermal electrons. *Chaos Solitons Fractals* **2003**, *18*, 849–853. [CrossRef]
18. Maharaj, S.K.; Pillay, S.R.; Bharuthram, R.; Reddy, R.V.; Singh, S.V.; Lakhina, G.S. Arbitrary amplitude dust-acoustic double layers in a non-thermal plasma. *J. Plasma Phys.* **2006**, *72*, 43–58. [CrossRef]
19. Baluku, T.K.; Hellberg, M.A. Plasma Physics and Controlled Fusion Ion acoustic solitary waves in an electron–positron–ion plasma with non-thermal electrons. *Plasma Phys. Control. Fusion* **2011**, *53*, 095007. [CrossRef]
20. Verheest, F.; Pillay, S.R. Large amplitude dust-acoustic solitary waves and double layers in nonthermal plasmas. *Phys. Plasmas* **2008**, *15*, 013703. [CrossRef]
21. Verheest, F.; Hellberg, M.A. Compressive and rarefactive solitary waves in nonthermal two-component plasmas. *Phys. Plasmas* **2010**, *17*, 102312. [CrossRef]
22. Tsallis, C. Generalized entropy-based criterion for consistent testing. *Phys. Rev. E* **1998**, *58*, 1442. [CrossRef]
23. Lima, J.A.; Silva, R., Jr.; Santos, J. Plasma oscillations and nonextensive statistics. *Phys. Rev. E* **2000**, *61*, 3260. [CrossRef]
24. Jacquinot, J.; McVey, B.D.; Scharer, J.E. Mode conversion of the fast magnetosonic wave in a deuterium-hydrogen tokamak plasma. *Phys. Rev.* **1977**, *39*, 88. [CrossRef]
25. Sauer, K.; McKenzie, J.F.; Dubinin, E. Waves and nonlinear structures in bi-ion plasmas. In *AIP Conference Proceedings*; American Institute of Physics: College Park, MD, USA, 2000; Volume 537, pp. 327–339.
26. Lonngren, K.E. Soliton experiments in plasmas. *Plasma Phys.* **1983**, *25*, 943–982. [CrossRef]
27. Ichiki, R.; Shindo, M.; Yoshimura, S.; Watanabe, T.; Kawai, Y. Ion acoustic waves in one-and two-negative ion species plasmas. *Phys. Plasmas* **2001**, *8*, 4275–4283. [CrossRef]
28. Ichiki, R.; Yoshimura, S.; Watanabe, T.; Nakamura, Y.; Kawai, Y. Experimental observation of dominant propagation of the ion-acoustic slow mode in a negative ion plasma and its application. *Phys. Plasmas* **2002**, *9*, 4481–4487. [CrossRef]
29. Nakamura, Y.; Nakamura, M.; Itoh, T. Observation of two ion-acoustic waves in an argon-helium plasma. *Phys. Rev. Lett.* **1976**, *37*, 209. [CrossRef]
30. Wong, A.Y.; Mamas, D.L.; Arnush, D. Negative ion plasmas. *Phys. Fluids* **1975**, *18*, 1489–1493. [CrossRef]
31. Nakamura, Y.; Bailung, H.; Lonngren, K.E. Oblique collision of modified Korteweg–de Vries ion-acoustic solitons. *Phys. Plasmas* **1999**, *6*, 3466–3470. [CrossRef]
32. Amemiya, H.; Annaratone, B.M.; Allen, J.E. The double sheath associated with electron emission into a plasma containing negative ions. *J. Plasma Phys.* **1998**, *60*, 81–93. [CrossRef]

33. Vyas, V.; Hebner, G.A.; Kushner, M.J. Self-consistent three-dimensional model of dust particle transport and formation of Coulomb crystals in plasma processing reactors. *J. Appl. Phys.* **2002**, *92*, 6451–6460. [CrossRef]
34. Franklin, R.N. The plasma-wall boundary region in negative-ion-dominated plasmas at low pressures. *Plasma Sources Sci. Technol.* **2000**, *9*, 191. [CrossRef]
35. Abid, A.A.; Rehman, M.; Khan, M.Z.; Sarfraz, Z.; Lu, Q. The influence of multi-ion streaming on the variation of dust particle surface potential with Maxwellian/non-Maxwellian dusty plasmas. *Phys. Plasmas* **2017**, *24*, 083702. [CrossRef]
36. Williams, G.; Kourakis, I.; Verheest, F.; Hellberg, M.A. Re-examining the Cairns-Tsallis model for ion acoustic solitons. *Phys. Rev. E* **2013**, *88*, 023103. [CrossRef]
37. Tribeche, M.; Amour, R.; Shukla, P.K. Ion acoustic solitary waves in a plasma with nonthermal electrons featuring Tsallis distribution. *Phys. Rev. E* **2012**, *85*, 037401. [CrossRef] [PubMed]
38. Rubab, N.; Murtaza, G. Dust-charge fluctuations with non-Maxwellian distribution functions. *Phys. Scr.* **2006**, *73*, 178. [CrossRef]